August, 1996

Effects of Strong Interaction on the Electromagnetic Dissociation

A. MÜNDEL and G. BAUR

IKP (Theorie), Forschungszentrum Jülich, D-52425 Jülich, Fed. Rep. Germany.

Abstract

We investigate effects of strong interactions on the electromagnetic dissociation of nuclei in heavy ion collisions.

We start from the eikonal approach to the equivalent photon method to describe the electromagnetic contributions to the cross section of peripheral collisions. We summarize some results of this approach and characterize recent experiments in "universal plots".

In the second part of this work, we give a straight forward method to include transitions induced by the strong interactions between the ions. We introduce different methods to obtain the nuclear transition potential, and study the behavior of the resulting nuclear contributions.

1 Introduction

The Coulomb field of a fast moving heavy ion is an intense source of quasi real photons [1, 2, 3]. With raising projectile energy this photon spectrum becomes harder and there exist a variety of applications in nuclear– as well as astrophysics, like the excitation of giant resonances or the Coulomb dissociation of the ions [4].

The advantage of using heavy ions to study this processes are the large cross section, which make the Coulomb dissociation an interesting tool to study even multi–phonon resonances [5, 6] or the astrophysical S–factor for reactions like $^7Be(p,\gamma)^8B$ [4]. In the latter case phase-space considerations and the large number of equivalent photons highly favor the Coulomb dissociation compared to the direct measurement of the radiative capture reaction [7, 8].

A powerful but simple tool to describe the Coulomb dissociation of heavy ions is the equivalent photon method [3]. On the other hand this simple approach does not take into account excitations due to the strong interaction. Therefore it is interesting and necessary to study these effects. Using the hydro-dynamical model of Bohr and Tassie for the nuclear transition densities or potentials [9], one can connect the nuclear interaction to the optical potential and the deformation parameter and therefore to the electromagnetic transition matrixelements. This approach allows us to study these contributions in various cases of physical interest.

2 Equivalent photon spectrum in a Glauber approach

In the following we consider a situation where a projectile (particle 1) with charge Z_1 excites a target (particle 2) with charge Z_2 from a state $|I_i = 0, M_i = 0\rangle$ to the excited state $|I, M\rangle$ in a peripheral collision via the exchange of one quasi real photon of energy $E_\gamma = \hbar\omega$. The velocity $\vec{\beta} = \frac{\vec{v}}{c}$ of the projectile is in z direction and we use $\gamma = (1-\beta^2)^{-\frac{1}{2}}$.

The scattering angle of the projectile is denoted by θ. The inelastic scattering amplitude in the eikonal approximation $f(\theta)$ is than given by [10, 11]:

$$f(\theta) = \frac{ik}{2\pi\hbar v} \int d^3r \; d^3r' \; e^{i\vec{q}\cdot\vec{r}} \; e^{i\chi(b)} \langle \Phi_f(\vec{r}') | V_{int}(\vec{r}, \vec{r}') | \Phi_i(\vec{r}') \rangle, \tag{1}$$

where $\vec{q}$ denotes the momentum transfer and k is the wavenumber of the incoming projectile. We define $\vec{r}$ to be the separation of the centers of mass of the two nuclei, and $\vec{r}'$ to be the intrinsic coordinate of the target nucleus.

The Glauber phase $\chi(b)$ is the sum of a Coulomb and a nuclear part. If we assume the 'sharp cut–off' model for the nuclear part

$$e^{i\chi_N(b)} = \begin{cases} 0 & \text{if } b \leq R = R_1 + R_2 \\ 1 & \text{if } b > R \end{cases}, \tag{2}$$

where $R_i = 1.2 \; fm \; A^{1/3}$, $(i = 1, 2)$ is the radius of the i'th nucleus, the Coulomb phase is given by

$$\chi_C(b) = 2 \; \eta \; ln(kb). \tag{3}$$

Here $\eta = \frac{Z_1 Z_2 e^2}{\hbar v}$ is the Sommerfeld parameter.

Using standard methods [3] and defining the reduced electromagnetic transition probabilities $B(\pi l) = B(\pi l, I_i \to I_f)$ [12] we can write the cross section in the form

$$\frac{d\sigma}{d\Omega} = \sum_{\pi l} \int \frac{dE_\gamma}{E_\gamma} \; \sigma^{\pi l}_{E_\gamma}(E_\gamma) \; \frac{dn^{\pi l}}{d\Omega}. \tag{4}$$

In the above formula $\sigma^{\pi l}_\gamma(E_\gamma)$ is the photo-nuclear absorption cross section for a given multipolarity [3]

$$\sigma^{\pi l}_\gamma(E_\gamma) = \frac{(2\pi)^3(l+1)}{l[(2l+1)!!]^2} \rho_F(E_\gamma) \; (\frac{\omega}{c})^{2l-1} B(\pi l), \tag{5}$$

where $\rho_F(\omega)$ is the final state density.

Under these assumptions the equivalent photon number per unit solid angle for a given multipolarity $\frac{dn^{\pi l}}{d\Omega}$ is given by:

$$\frac{dn^{\pi l}_C}{d\Omega} = Z_1^2 \alpha \left(\frac{\omega k}{\gamma v}\right)^2 \frac{l[(2l+1)!!]^2}{(2\pi)^3(l+1)} \sum_m \left| G_{\pi l m}\left(\frac{1}{\beta}\right) \right|^2 |\Omega^C_m(q_T)|^2, \tag{6}$$

Here the transverse momentum transfer $q_T \approx k\theta$ is the only quantity, which depends on the scattering angle. Defining the variables

$$\begin{aligned} x = \frac{b}{R} \quad &; \quad \xi = \frac{\omega R}{\gamma v}; \\ \Theta_{diff} = \frac{1}{kR} \quad &; \quad \theta_{gr} = 2\eta\theta_{diff}, \end{aligned} \tag{7}$$

Ω_m^C can be written as:

$$\Omega_m^C(\theta) = R^2 \int_1^\infty x \; dx J_m(\frac{\theta x}{\theta_{diff}}) K_m(\xi x) \; e^{2i\eta ln(\frac{x}{\theta_{diff}})}. \tag{8}$$

In the case of the classic trajectory of the projectile ($\eta \to \infty$), one can use the saddle points method to solve the integral in eq. (8)[11]:

$$\Omega_m^{sc}(\theta) = R^2 \frac{y^2}{2\eta} \; e^{i\tilde{\phi}} \; K_m(\xi y) \; , \tag{9}$$

where the variables $y = \frac{\theta_{gr}}{\theta}$ and $\tilde{\phi} = \frac{1}{2}\pi(m+1) + 2\eta\left(ln\left(\frac{2\eta}{\theta}\right) - 1\right)$ where introduced.

Expression (eq. 8) for Ω_m mainly depends on two parameters, the interaction strength η and the adiabaticity parameter ξ, which is the ratio of impact time to transition time in a grazing collision.

It is interesting to compare $|2\eta\frac{\Omega_m}{R^2}|^2$ as a function of $\frac{\theta}{\theta_{gr}}$ for fixed ξ but different η as shown in the 'universal plots' in figs. (1) and (2). The thick solid line shows the semi classical limit according to eq. (9) while the dashed and dotted lines are the solutions of eq (8) for different values of η. At $\frac{\theta}{\theta_{gr}} = 1$ the semi classical limit drops to zero while the full solutions extend to higher angles. At small angles the full solution shows diffraction effects, but for a large interval of angles the full solution for sufficiently large η is a fast oscillating function around the semi classical limit (dotted line). Only for small η (dashed line) the full solution differs substantially from the semi classical limit.

For the above reason the semi classical solution for the inelastic scattering amplitude (eq. 1) provides in many relevant cases already a good description of the experimental situation. Fig. (3) classifies some existing experiments in a ξ–η–plot where the experiments well described by the semi classical solution are at large η and small ξ.

To complete the discussion of the sharp cut-off model we want to give the expression for the total cross section, which is obtained by integrating eq. (4) over the solid angle and using the closure relation for the Bessel functions. One finds:

$$\sigma_{tot} = 2\pi \left(\frac{Ze}{\hbar c}\right)^2 \left(\frac{\omega}{\gamma v}\right)^2 \sum_{\pi lm} \left(\frac{\omega}{c}\right)^{2(l-1)} |G_{\pi lm}(\frac{1}{\beta})|^2 B(\pi l) R^2 \int_1^\infty x\ dx\ K_m^2(\xi x). \qquad (10)$$

Notice, that this expression is independent of η.

3 The nuclear excitation part

The sharp cut–off model, as it was introduced in the last section, takes nuclear effects into account only in a very simplified way. A more realistic model for the nuclear contributions will influences the inelastic scattering amplitude (eq. 1) in two different ways. First it leads to an additional transition potential in eq. (1) of the form $\langle \Phi_f(\vec{r}\,')|V_N|\Phi_i(\vec{r}\,')\rangle$, where V_N is the nuclear potential between the two nuclei. In addition it will change the nuclear phase due to

$$\chi_N(b) = -\frac{1}{\hbar v} \int_{-\infty}^{\infty} V_N(\sqrt{b^2 + z^2}) dz, \qquad (11)$$

which, in contrast to the sharp cut–off model, now has a finite real and imaginary part. This leads to a "smoother" cut–off than in the sharp cut–off model and a modification of the Coulomb potential V_C due to the penetration of the two charge distributions. In the following we will neglect the effect on the Coulomb potential but keep eq. (11), and concentrate on the nuclear induced transitions.

There exist different approaches to obtain the nuclear transition potential (eq. 1) $\langle \Phi_f(\vec{r}\,')|V_N|\Phi_i(\vec{r}\,')\rangle$. In this work we assume a collective nuclear model.

First we want to describe the approach via the transition densities. In this case the nuclear transition potential can be calculated using the folding formalism [13]:

$$\langle \Phi_f(\vec{r}\,')|V_N(\vec{r},\vec{r}\,')|\Phi_i(\vec{r}\,')\rangle = \langle t_{NN}(E)\rangle\ \ \rho_1(\vec{r}-\vec{r}\,')\ \ \langle I, M|\rho_2(\vec{r}\,')|0,0\rangle\,. \qquad (12)$$

Here $\rho_i,\ (i = 1, 2)$ denotes the charge density of the i'th nucleus. For the energy dependent t_{NN}–matrix see ref. [13]. To determine the transition density matrix elements

$\langle I, M|\rho_2(\vec{r}\,')|0,0\rangle$ we assume the hydro-dynamical model of Bohr and Tassie [9]:

$$\langle I, M|\rho_2(\vec{r}\,')|0,0\rangle = \frac{\beta_I R_2^{2-I}}{\sqrt{2I+1}} r'^{(I-1)} \frac{d\rho_2(\vec{r}\,')}{dr'}\ Y^*_{IM}(\hat{r}\,'). \tag{13}$$

The deformation parameter β_l is related to the electromagnetic transition matrixelements $M(El,m)$ by:

$$M(El,m) = \sqrt{2l+1}\beta_l R_2^{2-l} \int_0^\infty dr\ r^{2l}\rho_2(r)\ \delta_{M,m} \tag{14}$$

Under these assumptions the inelastic scattering amplitude (eq. 1) can be written as:

$$\begin{aligned} f(\theta) = \ & \sum_{\pi lm} \ \frac{i^{m+1}k}{\hbar v}\ e^{-im\alpha}\ \langle I, M|M(\pi l,m)|0,0\rangle \\ & \int_0^\infty \ \ b\ db\ e^{i(\chi_C(b)+\chi_N(b))} J_m(q_T b)\ \left\{\Gamma_C^{\pi lm}(b) + \Gamma_N^{\pi lm}(b)\right\}, \end{aligned} \tag{15}$$

where α is the azimuthal scattering angle. Since we neglect the corrections of the Coulomb part due to the penetration of the two particles, $\Gamma_C^{\pi lm}$ is still assumed to be given by:

$$\Gamma_C^{\pi lm}(b) = \frac{Z_1 e}{\gamma}\ (\frac{\omega}{c})^l\ \sqrt{2l+1} G_{\pi lm}\left(\frac{1}{\beta}\right)\ K_m\left(\frac{\omega b}{\gamma v}\right). \tag{16}$$

For the sake of mathematical simplicity we consider a Gaussian shaped charge distribution for the two nuclei [13] to calculate $\Gamma_N^{\pi lm}$:

$$\rho_i(r) = \rho_i(0) e^{-\frac{r^2}{R_{G_i}^2}}\ ;\ \ \rho_i(0) = 0.085 fm^{-3} e^{\frac{R_i}{2a_i}}. \tag{17}$$

We have used the notation $R_{G_i}^2 = 2a_i R_i$, where a_i is the diffuseness parameter of the i'th nucleus. This choice for the charge distribution allows us to perform most of the calculations in an analytical way.

Under the above assumptions the nuclear phase (eq. 11) is given by [14]

$$\chi_N(b) = \langle t_{NN}(E)\rangle\ \ \rho_1(0)\ \rho_2(0) \left\{\frac{R_{G_1}^3 R_{G_2}^3}{R_G^2}\right\} e^{-b^2/R_G^2}, \tag{18}$$

where $R_G^2 = R_{G_1}^2 + R_{G_2}^2$. To take into account the singularity $\chi_C(b=0)$ (eq. 3), we modify the Coulomb phase [11]:

$$\chi_C(b) = 2\eta \left\{ ln(kb) + \frac{1}{2} E_1\left(\frac{b^2}{R_G^2}\right)\right\}. \tag{19}$$

In the above formula E_1 denotes the exponential integral.

Calculating the nuclear transition density as given in eq. (13) and using eq. (14) we find for $\Gamma_N^{\pi lm}(b)$:

$$\begin{aligned}\Gamma_N^{Elm}(b) &= \pi\,\frac{\rho_1(0)}{e}\,\frac{2^{l+2}}{(2l+1)!!}\,\frac{R_{G_1}^3}{R_G^{2l+3}}\,\langle t_{NN}(E)\rangle \\ &\quad \int dz\; r^l\; e^{i\frac{\omega}{v}z}\; e^{-\frac{r^2}{R_G^2}}\; Y_{lm}(\theta_{\hat{r}},0)\delta_{I,l}, \\ \Gamma_N^{Mlm}(b) &= 0. \end{aligned} \tag{20}$$

The Gauss parameterization for the charge densities is a relatively good approximation for light nuclei, but fails for heavy nuclei. Starting from more realistic densities immediately makes it necessary to solve the folding integral (eq. 12) numerically. To avoid these difficulties one can start from optical potential rather then their corresponding densities. This formalism is described in ref. [15].

For deformed optical potentials of the form $V_N(R(\theta,\phi),r)$, where $R(\theta,\phi) = R_0(1 + \sum_{\lambda\mu} a_{\lambda\mu} Y^*_{\lambda\mu}(\theta,\phi))$, that depend only on the distance $(R(\theta,\phi) - r)$, the nuclear transition potential $\langle I, M|V_N|0,0\rangle$ is of the form [18]

$$\langle I, M|V_N|0,0\rangle = \frac{-1}{\sqrt{2I+1}}\beta_I\; R_2 \frac{dV_N(R(\theta,\phi)-r)}{dr} Y^*_{IM}(\theta,\phi). \tag{21}$$

In both, the Tassie model and the Bohr Mottelson model [16], β_I is than given by

$$\beta_I = \frac{4\pi}{3}\frac{1}{Z_2 R_2^I}\sqrt{\frac{B(EI)}{e^2}}. \tag{22}$$

Using eqn. (21, 22, 15, and 1) we find for $\Gamma_N^{Elm}(b)$:

$$\Gamma_N^{Elm}(b) = \frac{-4\pi}{3Z_2 e R_2^{l-1}} \int dz\;\; e^{i\frac{\omega}{v}z}\; \frac{dV_N(R(\theta,\phi)-r)}{dr}\; Y_{lm}(\theta_{\hat{r}},0)\delta_{I,l}, \tag{23}$$

with $r^2 = b^2 + z^2$.

This result can be compared to the Distorted Wave Born Approximation (DWBA), see for example ref. [19]. In this formalism the nuclear part of the inelastic scattering amplitude for a transition from a state $|I_i = 0, M_i = 0\rangle$ to the exited state $|I, M\rangle$ is given

by

$$f^{DWBA}_{N,I,M}(\theta) = \frac{-2ik^2}{\hbar v}\sum_{\lambda}\sum_{\lambda',\mu'}\sqrt{4\pi}\; i^{\lambda-\lambda'}\; e^{i(\sigma_\lambda+\sigma_{\lambda'})}\sqrt{2\lambda'+1}\;\frac{R_2\beta_I}{\sqrt{2I+1}}\;\frac{1}{kk'}R^I_{\lambda\lambda'}$$
$$\sqrt{\frac{2I+1}{4\pi}}(\lambda'\;\mu'\;I\;M|\lambda\;0)(\lambda'\;0\;I\;0|\lambda\;0)\;Y_{\lambda'\mu'}(\theta,0), \qquad (24)$$

where k (k') is the wave number of the incoming (outgoing) wave. The radial matrixelement $R^I_{\lambda'\lambda}$ has the form [19]:

$$R^I_{\lambda\lambda'} = \int d^3r f_{\lambda'}(k'r)\frac{dV_N(R(\theta,\phi)-r)}{dR_0}f_\lambda(kr). \qquad (25)$$

For small scattering angles θ and large values for the angular momentum of the partial waves λ, λ' one can show that eq. (24) is equivalent to the derived Glauber approach (eqn. 15, 23).

This connection of the Glauber model to the DWBA can be seen as following. In eq. (25) the radial Coulomb wave function f_λ in the WKB approximation is given by [19, 20]

$$f_\lambda \approx e^{i\delta_\lambda}(k^2/g(r))^{\frac{1}{4}}sin\Phi \qquad (26)$$

where

$$\Phi = \frac{\pi}{4}+\int_{r_0}^{r}\sqrt{g(r)}\;dr$$
$$g(r) = k^2-\frac{2\eta k}{r}-\frac{\lambda(\lambda+1)}{r^2}\approx k^2-\frac{\lambda(\lambda+1)}{r^2} \qquad (27)$$

and r_0 is defined by $g(r_0)=0$.

Assuming $R^I_{\lambda'\lambda}\approx R^I_{\bar\lambda\bar\lambda}$ with $\bar\lambda=\frac{1}{2}(\lambda+\lambda')$ for sufficiently large values of λ one can follow the calculations from ref. [20], neglecting the rapidly scillating terms, and obtain

$$R^I_{\bar\lambda\bar\lambda} = e^{i\chi_N(b)}\frac{1}{4}\int_{-\infty}^{\infty}dz\; e^{i\frac{\omega}{v}z}\frac{dV_N(R(\theta,\phi),b,z)}{dR_0}, \qquad (28)$$

where we have used $e^{2i\delta_{\bar\lambda}} = e^{i\chi_N(b)}$ and neglected the Coulomb part in eq. (27), which leads to straight line trajectories instead of Rutherford trajectories. The $\bar\lambda$–dependence of $R^I_{\bar\lambda\bar\lambda}$ is contained in the impact parameter dependence of eq. (28), since one has $\bar\lambda+\frac{1}{2}\approx kb$. Making use of the approximation

$$Y_{\lambda'-M}(\theta,0)\approx\sqrt{\frac{2\lambda'+1}{4\pi}}J_M(kb\theta), \qquad (29)$$

in the limit of $\theta \ll 1$ and replace $\sum_\lambda \to k \int db$ on has

$$f^{DWBA}_{N,I,M}(\theta) = \frac{-ik}{\hbar v}\frac{2}{\sqrt{\pi}} R_2 \beta_I \int b\ db\ e^{i\chi_N(b)+\chi_C(b)} J_M(kb\theta) \sum_{\lambda'} i^{\lambda-\lambda'}(\lambda'\ -M\ I\ M|\lambda\ 0)(\lambda'\ 0\ I\ 0|\lambda\ 0)\frac{1}{4}\int_{-\infty}^{\infty} dz\ e^{i\frac{\omega}{v}z}\frac{dV_N(R(\theta,\phi),b,z)}{dR_0} \quad (30)$$

Here we have also identified $e^{i(\sigma_\lambda+\sigma_{\lambda'})} \approx e^{2i\sigma_{\bar{\lambda}}} = e^{i\chi_C(b)}$. Finally we make use of the approximation [19]

$$\sum_{\lambda'} i^{\lambda-\lambda'}(\lambda'\ -M\ I\ M|\lambda\ 0)(\lambda'\ 0\ I\ 0|\lambda\ 0) \approx i^{-M}\sqrt{\frac{4\pi}{2l+1}} Y_{IM}(\frac{\pi}{2},0), \quad (31)$$

for $(I+M)$ even and zero otherwise, and obtain for optical potentials $V_N(R(\theta,\phi),r)$ that depend only on $(R(\theta,\phi)-r)$

$$f^{DWBA}_{N,I,M}(\theta) = (-1)^M \frac{i^{M+1}k}{\hbar v}\frac{R_2\beta_I}{\sqrt{2I+1}}\int b\ db e^{i\chi(b)} J_M(kb\theta)\int_{-\infty}^{\infty} dz\ e^{i\frac{\omega}{v}z}\frac{dV_N(R(\theta,\phi),b,z)}{dr} Y_{IM}(\frac{\pi}{2},0). \quad (32)$$

This result is identical to eqn. (15, 23) for a surface peaked nuclear interaction ($Y_{IM}(\theta_{\hat{r}},0) \approx Y_{IM}(\frac{\pi}{2},0)$) apart from an overall phase, which doesn't influence the cross section.

We want to stress, that we made essential use of the assumption, that the angular momentum of the contributing partial waves λ and λ' are large, and that the cross section is limited to small scattering angles, which both are sufficiently fulfilled for most heavy ion collisions.

To apply eqn. (15, 23) for the nuclear contribution we want to assume a Woods–Saxon parameterization for the nuclear potential $V_N = U(r) + iW(r)$ where

$$U(r) = -U_0\left(e^{\frac{r-R_U}{a_U}}+1\right)^{-1}\ ;\ \ W(r) = -W_0\left(e^{\frac{r-R_W}{a_W}}+1\right)^{-1}. \quad (33)$$

In fig (4) we show the results with the above formalism for the Coulomb dissociation of ^8B. This reaction has recently been studied experimentally [21] in order to determine the astrophysical S–factor of the $^7B(p,\gamma)^8B$ reaction [17, 21]. The figure shows the cross section for a $51.9 MeV/nucleon$ ^8B beam on a ^{208}Pb target. The excitation energy is assumed to be $1.2 MeV$. The solid line shows the total cross section ($E1+E2$), the dashed line the sum of the Coulomb and nuclear contribution for $l=2$ ($E2_{C+N}$), and the dotted

line gives the $E2_N$ contribution only. We used $S_{17}(E1) = 20eVb$ and $S_{17}(E2) = 10meVb$. For the Woods–Saxon potential we assumed the following parameters [22],

$$\begin{aligned} U_0 = 50MeV \quad &; \quad W_0 = 57MeV \ ; \\ R_U = R_W = 8.5fm \quad &; \quad a_U = a_W = 0.8fm. \end{aligned} \tag{34}$$

One should bare in mind that the use of the collective model for this $^8B \rightarrow^7 Be + p$ continuum transition is not well justified. A diffraction dissociation approach would certainly be more appropriate, see e.g. ref. [23].

A more schematic model for the optical potential $V_N = U_N + iW_N$ is given by the "ramp" potential,

$$U(r) = \begin{cases} -U_0 & \text{if } r < R_U^- \\ -\frac{U_0}{\Delta_U}(R_U^+ - r) & \text{if } R_U^- \leq r \leq R_U^+ \\ 0 & \text{if } r > R_U^+ \end{cases} , \tag{35}$$

where $R_U^{\pm} = R_U \pm \frac{\Delta_U}{2}$. The imaginary part W_N is given in a similar way.

Fig. (5) compares the nuclear phase $|e^{i\chi_N(b)}|^2$ and $|\Gamma_N^{lm}(b)|^2$ for Woods–Saxon (solid line) and the "ramp" potential (dashed line). The functions where calculated at $\theta = 2.0^o$, for $l = 2$, $m = 0$, and are plotted as a function of b/R. For the Woods–Saxon potential we used $U_0 = 50MeV$, $W_0 = 57MeV$, $R_U = R_W = 8.5fm$, and $a_U = a_W = 0.8$ and the same parameters for the "ramp" potential but $\Delta_U = \Delta_W = 4fm$. One finds, that for an adequate choice of parameters both models give similar results.

Because the product $|e^{i\chi_N(b)}\Gamma_N^{lm}(b)|$ is a good measure for the nuclear transition strength, we want to deduce some basic features of this quantity. The magnitude of the real part U_0 is directly proportional to the magnitude of $|\Gamma_N^{lm}(b)|$, while the imaginary part W_N mainly influences the shape of $|e^{i\chi_N(b)}|^2$. Namely for decreasing W_0 the contributions for $b < R - \Delta_W$ in eq. (15) becomes important. This leads to an increasing nuclear contribution, while the oscillations of the Coulomb contribution around the semi classical limit (figs. 1 and 2) decrease. For the radii a choice like $R_U > R_W$ will lead to a larger overlap in fig. (5) and therefore to a larger value for $|e^{i\chi_N(b)}\Gamma_N^{lm}(b)|$.

This shows, that the magnitude of the nuclear contribution can vary over a wide range if one uses different sets of parameters for the optical potential.

For sufficiently large W_0 and small Δ one can deduce a very simple expression for the "ramp" model. For simplicity we assume $R_U = R_W = R$ and $\Delta_U = \Delta_W = \Delta$. The nuclear phase is then approximately given by

$$e^{i\chi_N(b)} = \begin{cases} 0 & \text{if } b < R_U^- \\ \frac{b-R^-}{\Delta} & \text{if } R_U^- \leq b \leq R_U^+ \\ 1 & \text{if } b > R_U^+ \end{cases} , \tag{36}$$

Using this approximations, we find for $e^{i\chi(b)}\Gamma_N^{Elm}(b)$:

$$\begin{aligned} e^{i\chi_N(b)}\Gamma_N^{Elm}(b) &= \frac{4\pi}{3Z_2eR_2^{l+1}}\frac{b-R^-}{\Delta^2}(U_0+iW_0) \\ & \quad Y_{lm}(\frac{\pi}{2},0)\frac{2v}{\omega}sin\left(\frac{\omega z_{max}}{v}\right)\ \delta_{I,l}, \end{aligned} \tag{37}$$

for $R_U^- \leq b \leq R_U^+$ and zero otherwise. In eq. (37) we used $Y_{lm}(\theta_{\hat{r}},0) \approx Y_{lm}(\frac{\pi}{2},0)$ and we have defined $z_{max} = \sqrt{R^{+2}-b^2}$.

Expanding the sinus for small arguments and introducing the variables $D = (R_1 - R_2)/R$, $x = b/R$, and $\delta = \Delta/R$ one can write eq. (37)

$$\begin{aligned} e^{i\chi_N(x)}\Gamma_N^{Elm}(x) &= \frac{8\pi}{3Z_2e}\frac{2^l}{R^{l-2}}\frac{U_0+iW_0}{(1-D)^{l+1}}\frac{1}{\delta}\ Y_{l,m}(\frac{\pi}{2},0) \\ & \quad (x-1+\delta)\sqrt{(1+\frac{\delta}{2})^2-x^2}\ \delta_{I,l}. \end{aligned} \tag{38}$$

To see the influence of the parameters δ and D Fig. (6) shows $|f_N^{E22}(\theta)|^2$ obtained from eq. (37)as a function of θ/θ_{gr} for different values of δ (solid line $\delta = 0.5$, dashed line $\delta = 0.1$ and dotted line $\delta = 0.02$). We used $D = 0.5$, $\xi = 0.1$ and $\eta = 9$. Fig (7) shows the same for fixed $\delta = 0.5$ but varying D (solid line $D = 0.5$, dashed line $D = 0.3$ and dotted line $D = 0$).

We want to stress, that $\Gamma_N^{Elm}(b)$ is nearly independent from the excitation energy ω, while $\Gamma_C^{Elm}(b)$ decreases with increasing excitation energy due to the behavior of $K_m\left(\frac{\omega b}{\gamma v}\right)$ (eq. 16).

Finally we want to discuss the limit of the sharp cut–off model for the nucleus in the adiabatic limit ($k' = k$). In this limit eq. (28) becomes

$$R^I_{\bar{\lambda}\bar{\lambda}}(k' = k) = e^{i\chi_N(b)} \frac{1}{4} \int_{-\infty}^{\infty} dz \; \frac{dV_N(R(\theta,\phi), b, z)}{dR_0}, \tag{39}$$

and one can derive a relation between this radial matrixelement and the nuclear phase $e^{i\chi_N(b)}$

$$R^I_{\bar{\lambda}\bar{\lambda}}(k' = k) = \frac{i\hbar v}{4} \frac{de^{i\chi_N(b)}}{dR_0}, \tag{40}$$

where $e^{i\chi(b)}$ is like the optical potential $V_N(R(\theta,\phi), r)$ a function of the distance $(R(\theta,\phi) - r)$. Using eq. (2) for the nuclear phase, one finds for the sharp cut–off model

$$f_{N,I,M}(\theta) = i^M \; e^{-iM\alpha} \; \beta_I \; k \; R_2 \; R \; e^{i\chi_C(R)} \; Y_{LM}(\frac{\pi}{2}, 0) \; J_M(q_T R). \tag{41}$$

Using the asymptotic expansion for the Bessel function for large $q_T R$ one finds the typical oscillatory behavior for the nuclear contribution as predicted by Blair [19].

Fig. 8 compares the results for the E2 nuclear cross section for the different models for the same experiment as in Fig. 4. ($51.9 MeV/nucleon$ ^8B beam on a ^{208}Pb target). The solid line shows the result according to eq. (23) for a Woods–Saxon optical potential with the parameters as given in (34). The dashed line shows the result for the ramp model with $U_0 = 50 MeV$, $W_0 = 57 MeV$; $R_U = R_W = 8.5 fm$ and $\Delta_U = \Delta_W = 4 fm$ and the dotted line shows the result for the sharp cut–off model (eq. 41). The sharp cut–off result shows the typical Frauenhofer diffraction while both other models show a smoother nuclear contribution and a phase shift at higher scattering angles as compared to the sharp cut–off model due to the diffuse edge of the optical potential.

4 Conclusions

In the first part we discussed the pure Coulomb contribution in heavy ion collisions using the Glauber approach. Using so called "universal plots", it is possible, to characterize this Coulomb contributions to peripheral heavy ion collisions for different experiments.

The relevant parameters are the interaction strength η, the adiabaticity parameter ξ, and θ/θ_{gr}. It turns out, that for many experiments a semi-classical approach to the equivalent photon method is already a sufficiently good description of the data.

In the second part, we could include the nuclear excitation in a straight forward way. We used the folding formalism and the optical potential model, to determine the nuclear transition potential. The latter result was compared to the DWBA formalism. The introduction of the simplified "ramp" model makes it possible to clarify the role of the parameters of the used optical potentials.

A comparison of the sharp cut–off model results with results obtained from different parameterisations of the optical potential shows, that the nuclear contribution can be described within the discussed frameworks. Therefore the introduced model for the nuclear contribution makes it possible to estimate the nuclear effects on the electromagnetic Excitation and Dissociation of nuclei.

Acknowledgment

We want to thank Tohru Motobayashi and Stefan Typel for interesting discussions.

References

[1] C.F. Weizäcker, *Z. Phys.* **88** (1934) 612.

[2] E.J. Williams, *Phys. Rev.* **45** (1934) 729.

[3] C.A. Bertulani and G. Baur, *Phys. Rep.***163** (1988) 299.

[4] G. Baur and H. Rebel, *J. Phys. G* **20** (1994) 1.

[5] T. Aumann, C.A. Bertulani and K. Sümmerer *Phys. Rev.* **C 51** (1995) 416.

[6] H. Emling *Prog. Part. Nucl. Phys.* **33** (1994) 729.

[7] S. Typel and G. Baur, *Phys. Rev.* **C 50** (1994) 2104.

[8] H. Esbensen and G.F.Bertsch, *Phys. Lett.* **B 359** (1995) 13.

[9] L.J. Tassie, *Austral. J. Phys.***9**(1956)407.

[10] R.J. Glauber, *Lectures in theoretical Physics I* (Interscience Publishers, Inc., New York 1959).

[11] C.A. Bertulani and A.M. Nathan *Nucl. Phys.* **A 554** (1993) 158.

[12] K. Alder and A. Winther, *Electromagnetic Excitation* (North Holland, Amsterdam, 1965).

[13] A.N.F. Aleixo and C.A. Berulani *Nucl. Phys.* **A 528** (1991) 436.

[14] P.J. Karol, *Phys. Rev.* **C 11** (1975) 1203.

[15] G.R. Satchler *Nucl. Phys.* **A 472** (1987) 215.

[16] A.Bohr and B.R. Mottelson, *Nuclear Structure*, Vol. 2 (Benjamin, New York, 1971)

[17] T. Motobayashi et al., *Phys. Rev. Lett.* **73** (1994) 2680.

[18] G.R. Satchler, *Direct Nuclear Reactions* (Clarendon Press, Oxford, 1983).

[19] J. S. Blair, *Lectures in Theoretical Physics, Vol VIII-C*, (The University of Colorado Press, Boulder, 1966).

[20] K. Alder, A. Bohr, T. Huus, B. Mottelson, and A. Winther *Rev. of Mod. Phys.* **28** (1956) 432.

[21] T. Motobayashi, *Contribution to 'Nuclei in the Cosmos VI'*,Notre Dame 1996; proceedings to be published in *Nucl. Phys.* **A**

[22] J. Barrette et al., *Phys. Lett.* **B 209** (1988) 182.

[23] K. Hencken, G. Bertsch, and H. Esbensen, *Preprint nucl-th/9607049*.

Figure Captions

Figure 1: $|2\eta\frac{\Omega_0}{R^2}|^2$ for $\xi = 0.5$, $\eta = 20$ (dashed) and $\eta = 2$ (dotted) upper picture and for $\xi = 0.1$, $\eta = 3$ (dashed) and $\eta = 1.2$ (dotted) lower one. The solid line shows the result for the semi classical expression (eq. 9).

Figure 2: Same as fig. (1) but for $m = 2$

Figure 3: Some experiments characterized in a ξ–η–plot.

Figure 4: Cross section for the Coulomb dissociation of $51.9 MeV/nucleon$ ^8B beam on a ^{208}Pb target. The solid line shows the total cross section, while the dashed gives the $E2_{C+N}$, and the lower line only the $E2_N$ contribution

Figure 5: $|\Gamma_N^{E10}(b)|^2$ (left hand side) and $|e^{i\chi_N(b)}|^2$ (right hand side) as a function of $\frac{b}{R}$. The solid and the dashed line belong to the Woods–Saxon model and the simplified ramp model respectively.

Figure 6: $|f_N^{E22}(\theta)|^2$ as a function of θ/θ_{gr} for different values of δ (solid line $\delta = 0.5$, dashed line $\delta = 0.1$ and dotted line $\delta = 0.02$)

Figure 7: $|f_N^{E22}(\theta)|^2$ as a function of θ/θ_{gr} for different values of D (solid line $D = 0.5$, dashed line $D = 0.3$ and dotted line $D = 0$).

Figure 8: E2 nuclear cross section for the various models with the same experiment as in fig. 4. The solid line shows the result according to eq. (23) for a Woods–Saxon Potential, the dashed line for the ramp model and the dotted line for the sharp cut–off model (eq. 41). The parameters used for each potential are given in the text.

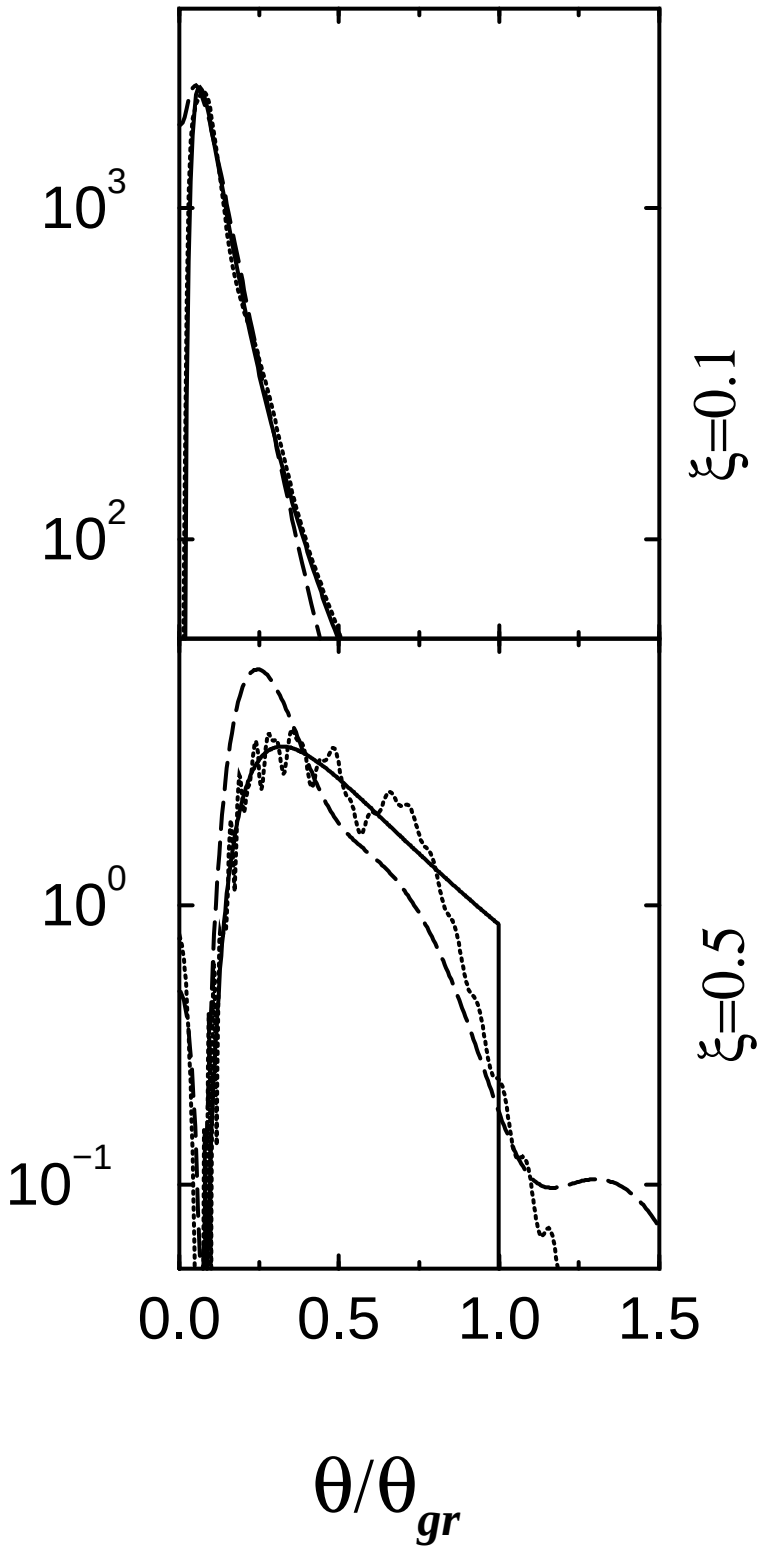
m = 0
10^3
10^2
10^0
10^−1
ξ=0.1
ξ=0.5
0.0
0.5
1.0
1.5
θ/θ_gr

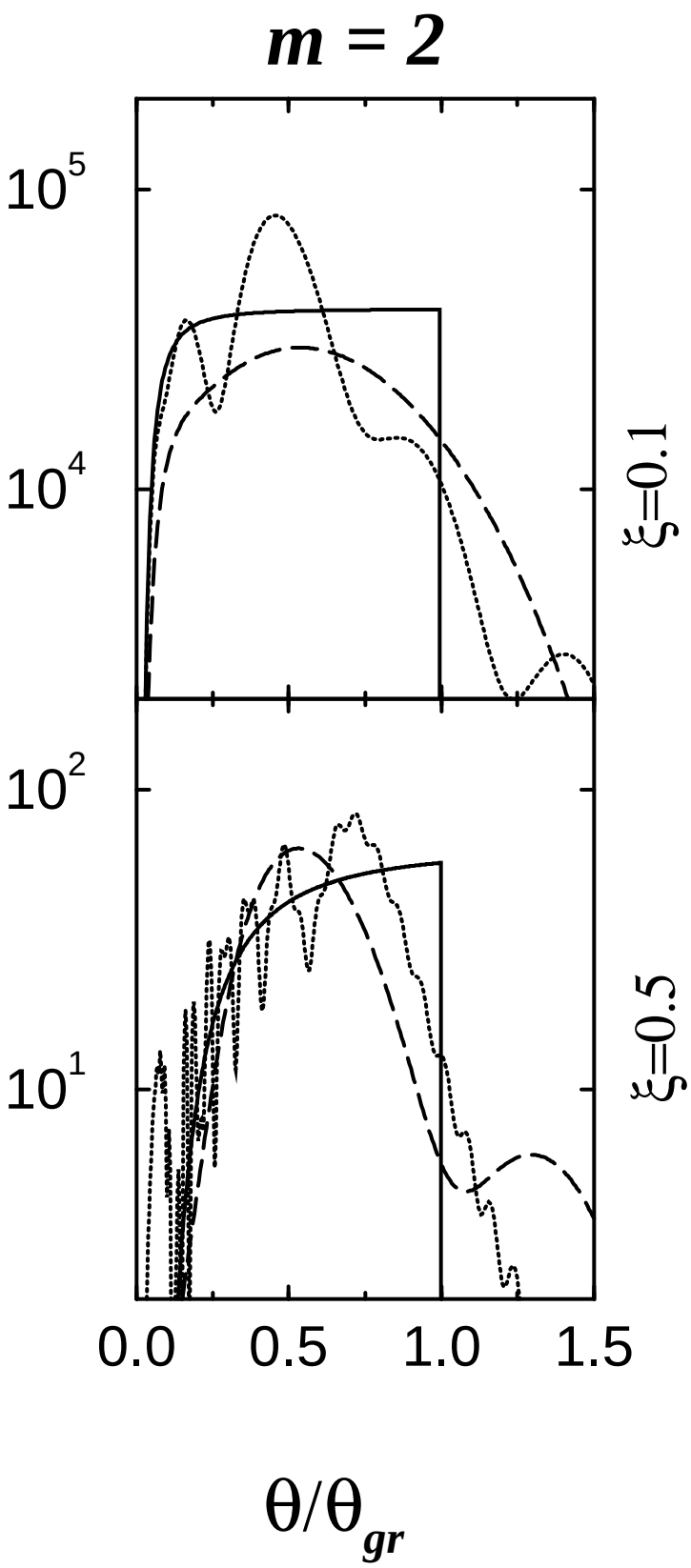
m = 2
10^5
10^4
10^2
10^1
ξ=0.1
ξ=0.5
0.0
0.5
1.0
1.5
θ/θ_gr

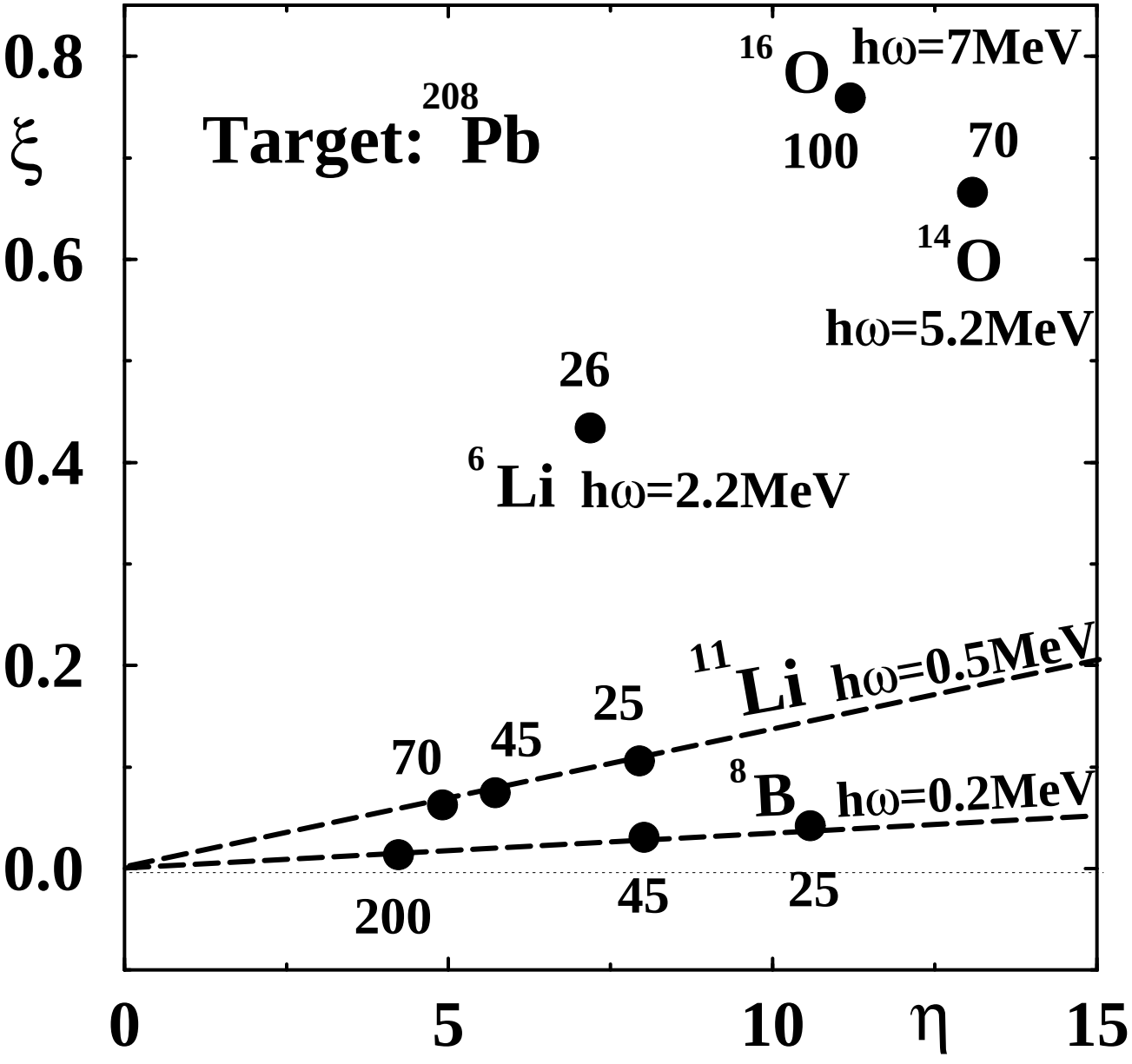
0.8
0.6
0.4
0.2
0.0
ξ
Target: 208Pb
16O hω=7MeV
100
70
14O
hω=5.2MeV
26
6Li hω=2.2MeV
11Li hω=0.5MeV
25
70
45
8B hω=0.2MeV
200
45
25
0
5
10
η
15

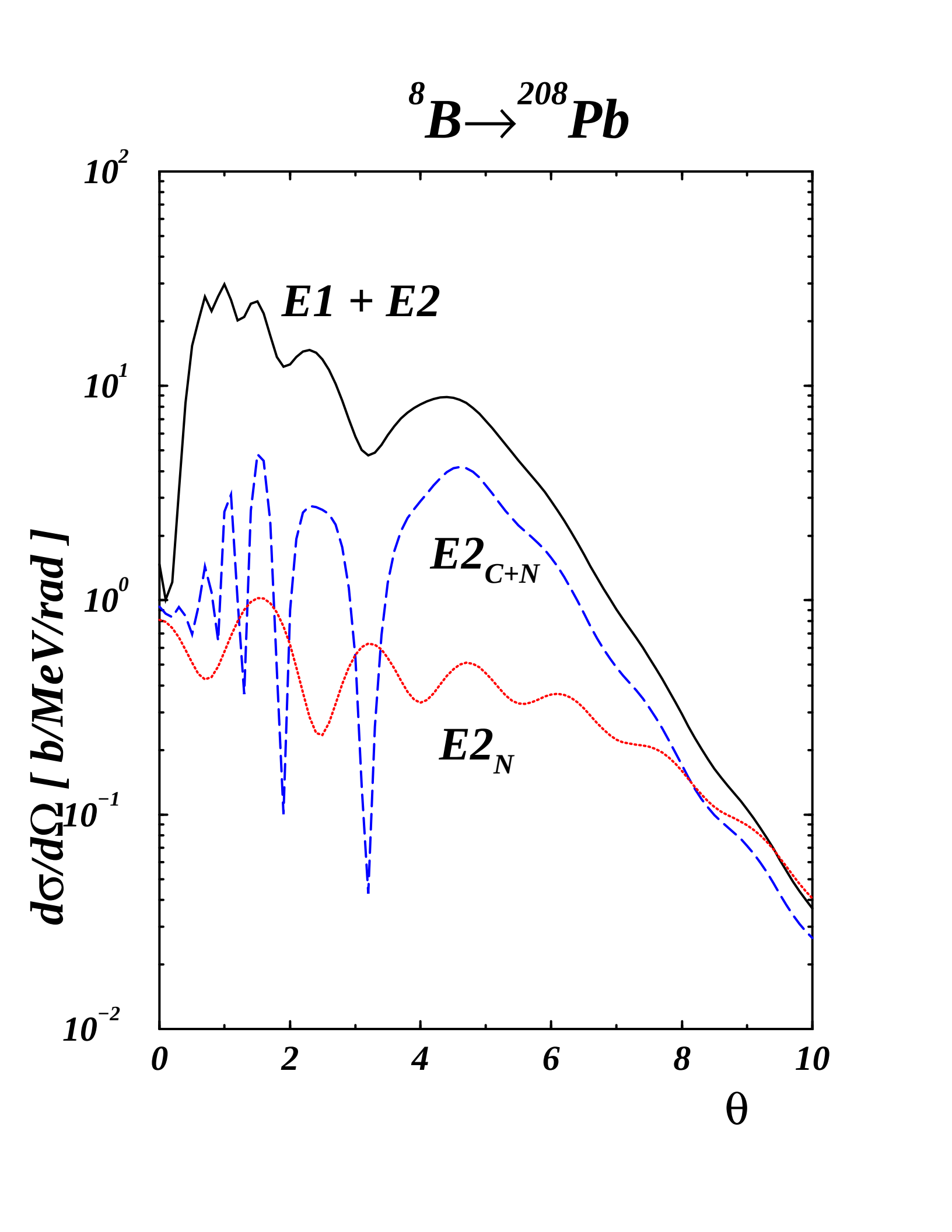
$^{8}B \rightarrow {}^{208}Pb$
10^{2}
10^{1}
10^{0}
10^{-1}
10^{-2}
E1 + E2
$E2_{C+N}$
$E2_{N}$
$d\sigma/d\Omega$ [b/MeV/rad]
0
2
4
6
8
10
θ

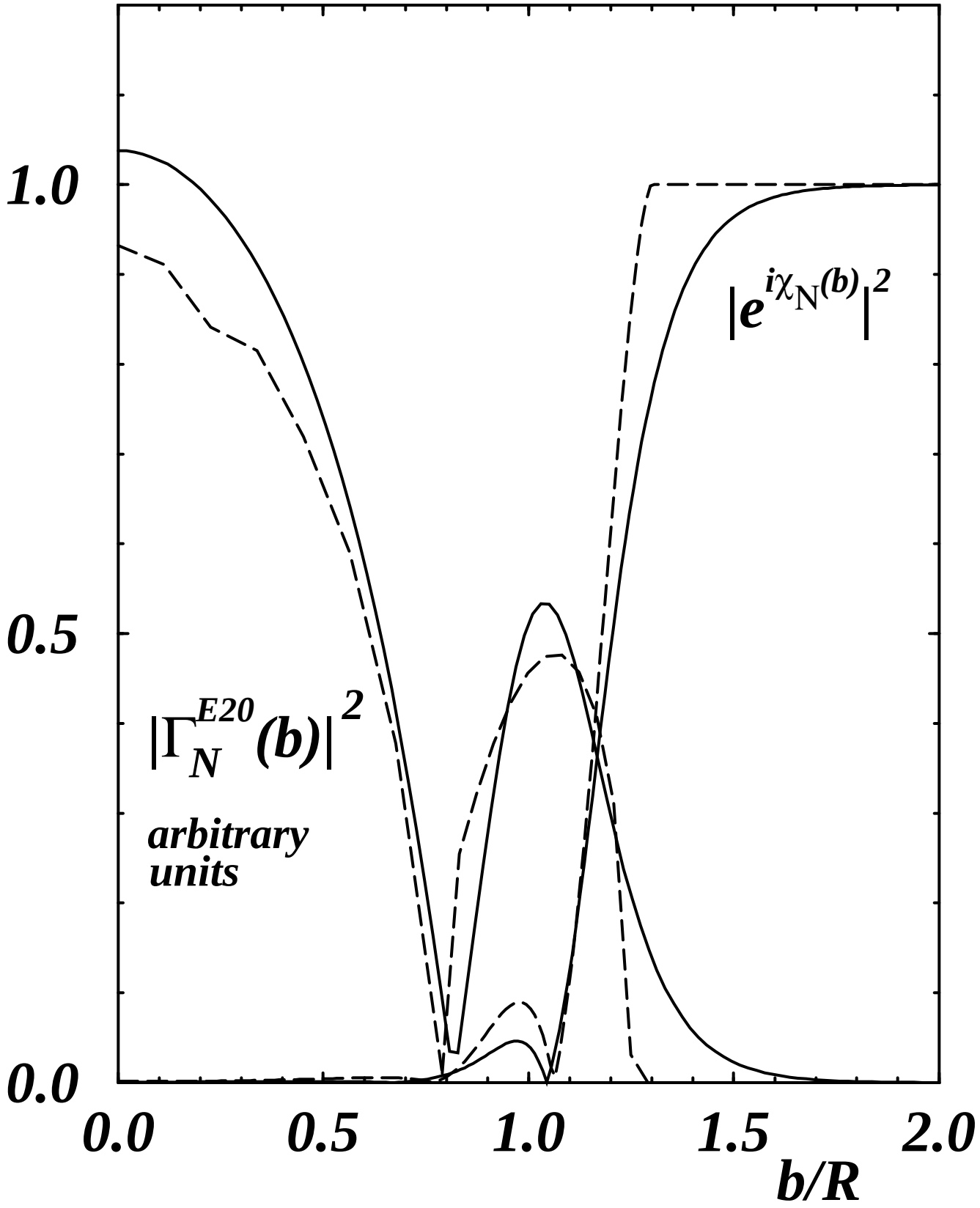
1.0
0.5
0.0
0.0
0.5
1.0
1.5
2.0
b/R
$|e^{i\chi_N(b)}|^2$
$|\Gamma_N^{E20}(b)|^2$
arbitrary
units

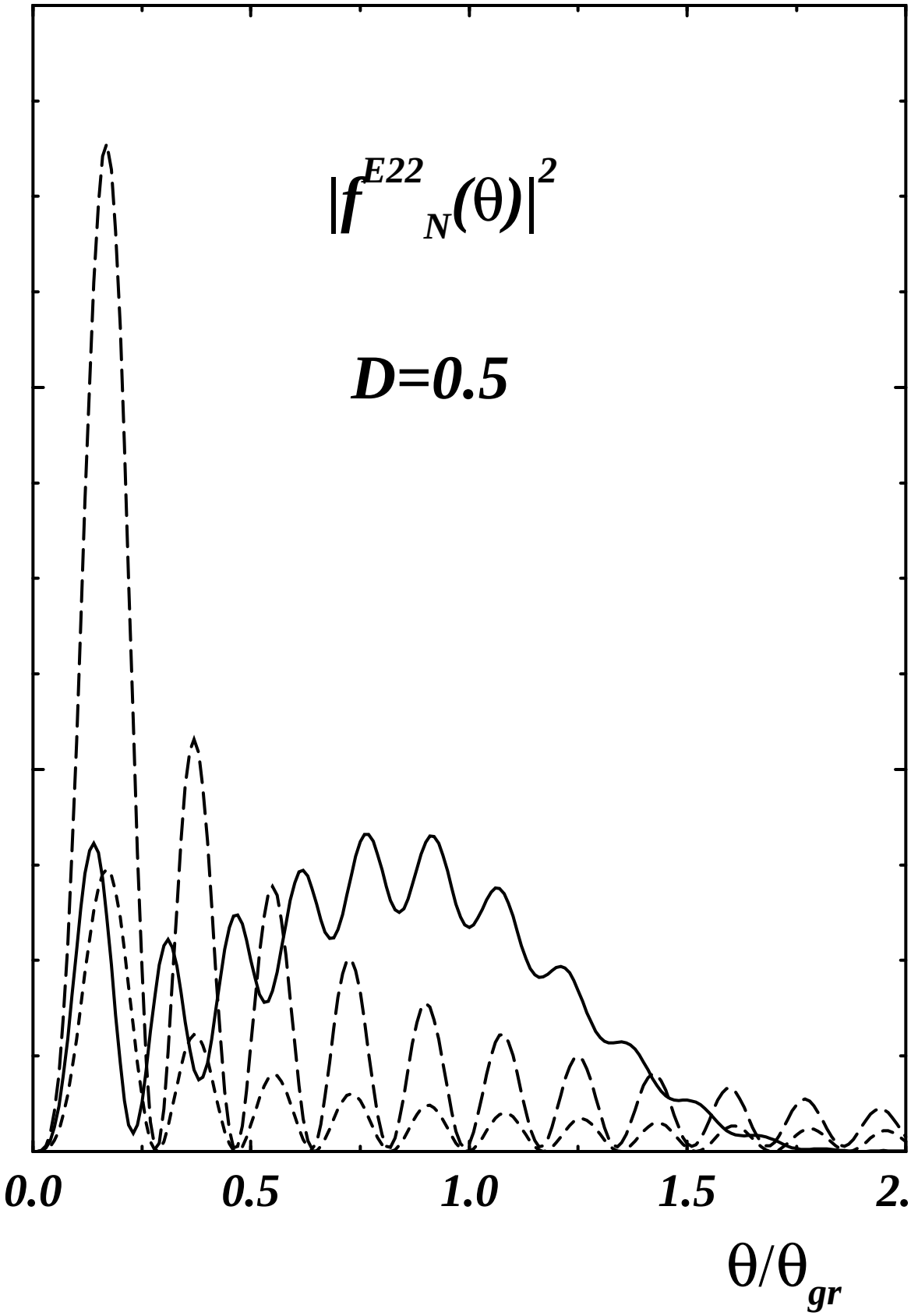
$|f^{E22}_{N}(\theta)|^2$
D=0.5
0.0
0.5
1.0
1.5
2.0
θ/θgr

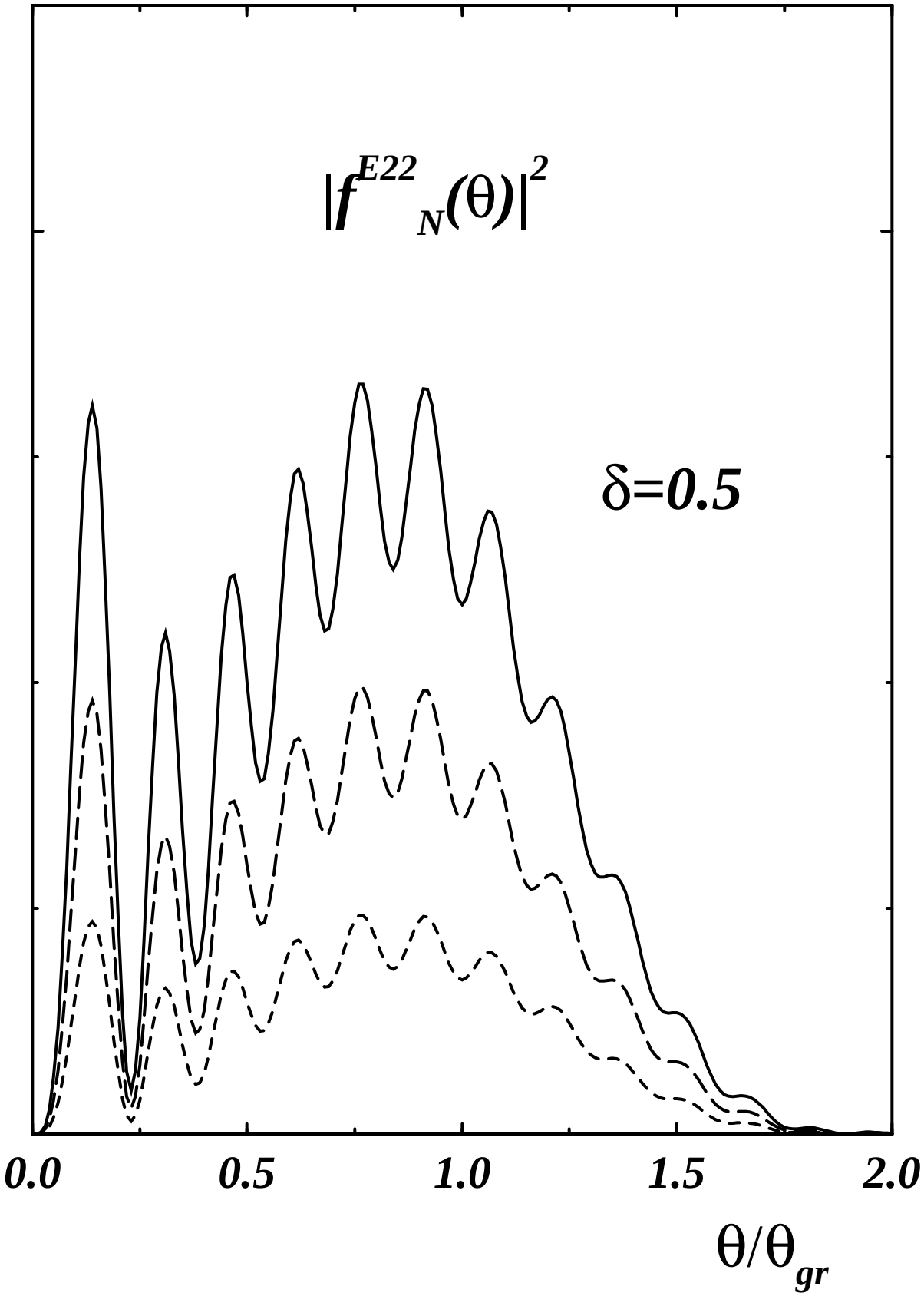
$|f^{E22}_{N}(\theta)|^2$
δ=0.5
0.0
0.5
1.0
1.5
2.0
θ/θ_gr

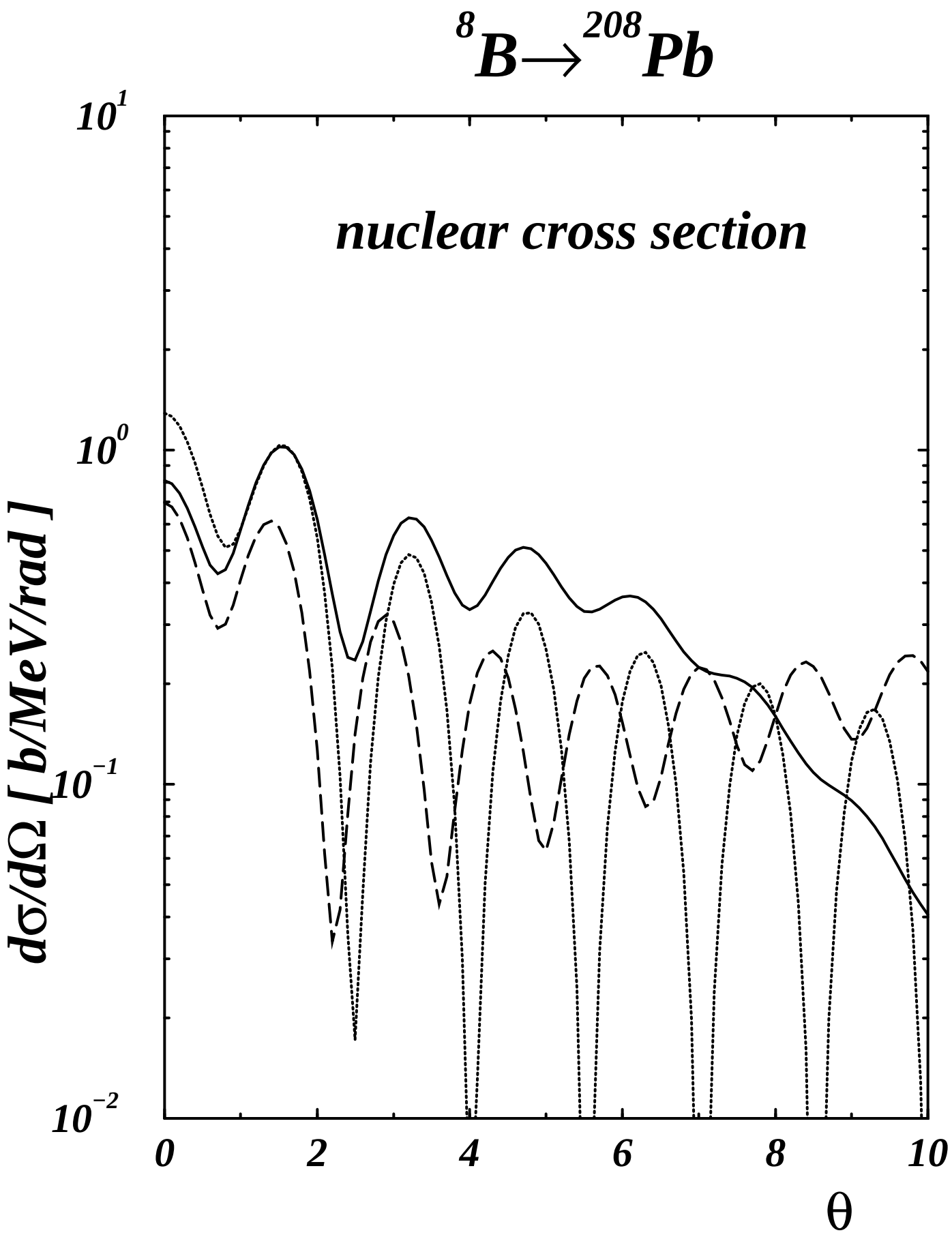
$^{8}B \rightarrow {}^{208}Pb$
nuclear cross section
10^{1}
10^{0}
10^{-1}
10^{-2}
$d\sigma/d\Omega$ [b/MeV/rad]
0
2
4
6
8
10
θ